Publication Year	2018
Acceptance in OA	2020-09-29T08:41:34Z
Title	A possible solution of the puzzling variation of the orbital period of MXB 1659-298
Authors	Iaria, R., Gambino, A. F., Di Salvo, T., Burderi, L., Matranga, M., Riggio, A., SANNA, ALBERTO, Scarano, F., D'AI', ANTONINO
Publisher's version (DOI)	10.1093/mnras/stx2529
Handle	http://hdl.handle.net/20.500.12386/27511
Journal	MONTHLY NOTICES OF THE ROYAL ASTRONOMICAL SOCIETY
Volume	473

Monthly Notices
of the
ROYAL ASTRONOMICAL SOCIETY

MNRAS **473,** 3490–3499 (2018) doi:10.1093/mnras/stx2529

A possible solution of the puzzling variation of the orbital period of MXB 1659–298

R. Iaria,[1]★ A. F. Gambino,[1] T. Di Salvo,[1] L. Burderi,[2] M. Matranga,[1] A. Riggio,[2] A. Sanna,[2] F. Scarano[2] and A. D'Aì[3]

[1]*Dipartimento di Fisica e Chimica, Università di Palermo, via Archirafi 36, I-90123 Palermo, Italy*
[2]*Dipartimento di Fisica, Università degli Studi di Cagliari, SP Monserrato-Sestu, KM 0.7, I-09042 Monserrato, Italy*
[3]*INAF/IASF Palermo, via Ugo La Malfa 153, I-90146 Palermo, Italy*

Accepted 2017 September 23. Received 2017 September 23; in original form 2016 November 21

ABSTRACT

MXB 1659–298 is a transient neutron-star low-mass X-ray binary system that shows eclipses with a periodicity of 7.1 h. MXB 1659–298 went to outburst in 2015 August, after 14 years of quiescence. We investigate the orbital properties of this source with a baseline of 40 years, obtained by combining the eight eclipse arrival times present in the literature with 51 eclipse arrival times collected during the last two outbursts. A quadratic ephemeris does not fit the delays associated with the eclipse arrival times and the addition of a sinusoidal term with a period of 2.31 ± 0.02 yr is required. We infer a binary orbital period of $P = 7.1161099(3)$ h and an orbital period derivative of $\dot{P} = -8.5(1.2) \times 10^{-12}$ s s^{-1}. We show that the large orbital period derivative can be explained with a highly non-conservative mass-transfer scenario, in which more than 98 per cent of the mass provided by the companion star leaves the binary system. We predict an orbital period derivative value of $\dot{P} = -6(3) \times 10^{-12}$ s s^{-1} and constrain the companion-star mass between 0.3 and 1.2 $M_{\odot}$. Assuming that the companion star is in thermal equilibrium, the periodic modulation can be due to either a gravitational quadrupole coupling arising from variations of the oblateness of the companion star or the presence of a third body of mass $M_3 > 21$ Jovian masses.

Key words: ephemerides – binaries: eclipsing – stars: individual: MXB 1659–298 – stars: neutron – X-rays: binaries – X-rays: stars.

1 INTRODUCTION

In low-mass X-ray binaries (LMXBs) with inclination angles between 75° and 80°, the X-ray emission may be totally shielded by the companion star. As the companion transits between the X-ray central source and the observer, the light curves show total eclipses. For inclination angles between 80° and 90°, the LMXB is observed as an accretion-disc corona (ADC) source. In this case, the observed X-ray emission comes from an extended corona that can reach the outer region of the accretion disc. The light curves of ADC sources show an almost sinusoidal modulation and partial eclipses. The modulation of the light curve is generally explained by the presence of a geometrically thick disc, the height of which varies with the azimuthal angle and occults part of the X-ray emission. Since the companion star does not shield the whole extended corona, the observed eclipses are partial; the prototype of ADC sources is X1822–371 (see e.g. Iaria et al. 2011, 2013, 2015a, and references therein).

Total eclipses represent a good time reference, which is ideal to perform timing analysis of the binary orbital period, e.g. the O−C method is usually applied to refine the orbital period or trace orbital period changes (see Chou 2014 for a recent review). To date, 12 LMXBs show total eclipses in their light curves. One of the best-studied eclipsing X-ray source is EXO 0748–676, as it was active for more than 20 years (see Wolff et al. 2009 and references therein).

The eclipsing LMXB MXB 1659–298 was discovered by Lewin et al. (1976). The light curve showed type-I X-ray bursts, thus revealing that the compact object was an accreting neutron star. The source was observed in outburst up to 1978 with *SAS3* and *HEAO* (Cominsky, Ossmann & Lewin 1983; Cominsky & Wood 1984, 1989). Eclipses were first reported by by Cominsky & Wood (1984), who estimated a periodicity of 7.1 h. Cominsky & Wood (1989) analysed two whole eclipses, estimating two eclipse arrival times. From 1978 up to 1999, the region containing MXB 1659–298 was monitored by the X-ray observatories on board *Hakucho*, *EXOSAT* and *ROSAT*, but the source was never detected (see Cominsky & Wood 1989; Verbunt 2001). During 1999 April, the Wide Field Cameras on board *BeppoSAX* observed the source in outburst again (in 't Zand et al. 1999). This new outburst continued

★ E-mail: rosario.iaria@unipa.it

© 2017 The Authors
Published by Oxford University Press on behalf of the Royal Astronomical Society

Downloaded from https://academic.oup.com/mnras/article/473/3/3490/4628110 by INAF Palermo (Osservatorio Astronomico di Palermo) user on 25 September 2020

up to 2001 September. During the outburst, MXB 1659–298 was observed with the Proportional Counter Array (PCA) on board the *Rossi X-ray Timing Explorer* (*RXTE*: see e.g. Wachter, Smale & Bailyn 2000), with the Narrow Field Instruments (NFI) on board *BeppoSAX* (Oosterbroek et al. 2001) and with *XMM–Newton*. From the analysis of the *RXTE* light curves of the source, Wachter et al. (2000) obtained four eclipse arrival times and found an orbital period derivative of $(-7.2 \pm 1.8) \times 10^{-11}$ s s^{-1}, suggesting that the orbit of the binary system is shrinking. Oosterbroek et al. (2001) obtained two eclipse arrival times from a *BeppoSAX*/NFI observation and, combining their data with those present in the literature, found that the orbital period derivative, $\dot{P}_{\rm orb}$, is positive, with a value of $(7.4 \pm 2.0) \times 10^{-12}$ s s^{-1}. MXB 1659–298 again went into outburst between 2015 August (Negoro et al. 2015) and 2017 April. Using data from the X-ray Telescope (XRT) on board *Swift*, Bahramian et al. (2016) observed that the unabsorbed flux in the 0.5–10 keV energy range was 1.5×10^{-10}, 4.6×10^{-10} and 2.2×10^{-10} erg cm^{-2} s^{-1} on 2016 January 28 and February 2 and 11, respectively.

Cominsky & Wood (1989) measured an eclipse duration, $\Delta T_{\rm ecl}$, of 932 ± 13 s and ingress/egress durations of $\Delta T_{\rm ing} = 41 \pm 13$ s and $\Delta T_{\rm egr} = 19 \pm 13$ s, respectively. They showed that, if the companion star is a main-sequence star of mass 0.9 M$_\odot$ with a temperature close to 5000 K, the scaleheight of the stellar atmosphere should be around 200 km, corresponding to an ingress/egress duration close to 0.5 s. The authors concluded that the small value of the scaleheight cannot justify the large values of measured ingress/egress durations. Furthermore, Cominsky & Wood (1989) suggested that the observed asymmetry between the ingress and egress durations could be caused by a one-sided extended corona of size 5×10^5 km^2.

From the analysis of four eclipses obtained with *RXTE*/PCA, Wachter et al. (2000) estimated an average eclipse duration of 901.9 ± 0.8 s and average values of ingress/egress durations of $\Delta T_{\rm ing} = 9.1 \pm 3.0$ s and $\Delta T_{\rm egr} = 9.5 \pm 3.3$ s. The authors proposed that the large spread of values associated with the ingress/egress times could be caused either by flaring activity of the companion star or by the presence of an evaporating wind from the surface of the companion star created by irradiation from the X-ray source.

Cominsky & Wood (1984) discussed the nature of the optical counterpart of MXB 1659–298, V2134 Oph, assuming an orbital period of 7.1 h and an eclipse duration of 900 s. They constrained the mass of the companion star to be between 0.3 M$_\odot$ and 0.9 M$_\odot$ for inclination angles of the binary system of 90° and 71°.5, respectively. Warner (1995) inferred that the companion-star mass is between 0.75 and 0.78 M$_\odot$ if the companion fills its Roche lobe. This range of masses suggests that the companion is a K0 main-sequence star. During the quiescence of MXB 1659–298, Wachter et al. (2000) measured a magnitude in the *I* band of 22.1 ± 0.3 mag and Filippenko et al. (1999) measured a magnitude in the *R* band of 23.6 ± 0.4 mag. Wachter et al. (2000) found that the value of $(R - I)_0$ is compatible with an early K spectral type. Moreover, they suggested that, for a companion star belonging to the K0 class, the visual magnitude should be $V = 23.6$ mag, a value that is compatible with the measured lower limit of $V > 23$ mag.

Galloway et al. (2008), analysing the type-I X-ray bursts observed with *RXTE*/PCA, inferred a distance to the source of 9 ± 2 and 12 ± 3 kpc for hydrogen-rich and helium-rich companion stars, respectively. Furthermore, Wijnands, Strohmayer & Franco (2001) detected nearly coherent oscillations with a frequency around 567 Hz during type-I X-ray bursts, suggesting that the neutron star could be an X-ray millisecond pulsar with a spin period of 1.8 ms.

The interstellar hydrogen column density, $N_{\rm H}$, was estimated by Cackett et al. (2008) during the X-ray quiescence of MXB 1659–298. Combining *Chandra* and *XMM–Newton* observations collected between 2001 and 2008, they fitted the X-ray spectrum, obtaining $N_{\rm H} = (2.0 \pm 0.1) \times 10^{21}$ cm^{-2}. Two more recent *Chandra* observations of the source, taken in 2012 (Cackett et al. 2013), seem to suggest an increase of the interstellar hydrogen column density up to a value of $(4.7 \pm 1.3) \times 10^{21}$ cm^{-2}. The authors proposed three different scenarios to explain the increase of $N_{\rm H}$: (a) material building up in the outer region of the accretion disc, (b) the presence of a precessing accretion disc and (c) sporadic variability during quiescence, due to low-level accretion.

Studying the *XMM*-Newton spectrum of MXB 1659–298, Sidoli et al. (2001) detected two absorption lines at 6.64 and 6.90 keV associated with the presence of highly ionized iron (Fe XXV and Fe XXVI ions), as well as absorption lines associated with highly ionized oxygen and neon (O VIII 1s–2p, O VIII 1s–3p, O VIII 1s–4p and Ne IX 1s–2p transitions) at 0.65, 0.77, 0.81 and 1.0 keV.

In this article, we report the updated ephemeris of MXB 1659–298, combining 45 eclipse arrival times obtained with *XMM–Newton* and *RXTE* during the outburst between 1999 and 2001 and six eclipse arrival times obtained with *XMM–Newton*, *NuSTAR* and *Swift*/XRT during the outburst starting in 2015. The available temporal baseline allows us to constrain the bizarre behaviour of the eclipse arrival times.

2 OBSERVATIONS

During the outburst occurred from 1999–2001, MXB 1659–298 was observed with *XMM–Newton* (Jansen et al. 2001) at two times: on 2000 March 22 and 2001 February 20. The latter observation (obsid. 0008620701) was analysed by Sidoli et al. (2001) and Díaz Trigo et al. (2006), who studied the spectral properties of the source during the persistent emission, the dip and the eclipse, while the former observation (obsid. 0008620601) was never analysed. During the 2015 outburst, MXB 1659–298 was observed with *XMM–Newton* on 2015 September 26.

The European Photon Imaging Camera (Epic-pn: Strüder et al. 2001) on board *XMM–Newton* collected data from the source in timing mode, with exposure times of 10, 32 and 34 ks, respectively. The Epic-pn light curve of the observation taken in 2001 shows two eclipses in the light curve (see fig. 1 of Sidoli et al. 2001). To verify the presence of eclipses in the Epic-pn light curves of the observations taken in 2000 and 2015, we filtered the source events with the Science Analysis System (SAS) version 15.0.0. We reprocessed the Epic-pn events and applied solar-system barycentre corrections, adopting as coordinates RA = 255°.527250 and Dec = −29°.945583 (see Wijnands et al. 2003). During the observation taken in 2000, the light curve of MXB 1659–298 shows an eclipse with a duration of 900 s approximately 1400 s after the start time. The count rate is 32 and 1.4 count s^{-1} outside and during the eclipse, respectively. During the observation taken in 2015, the light curve shows the presence of a type-I X-ray burst 12 ks after the start of the observation. The count rate varies from 32 count s^{-1} at the beginning of the burst up to 320 count s^{-1} at the peak. An intense dipping activity is present about 20 ks from the beginning of the observation, a complete eclipse is observed 26 ks from the start time and an eclipse without ingress is observed at the beginning of the observation. The count rate outside and during the eclipse is 32 and 1.4 count s^{-1}, respectively.

The PCA instrument on board *RXTE* (Jahoda et al. 1996) observed the source several times from 1999–2001. In our analysis,

Downloaded from https://academic.oup.com/mnras/article/473/3/3490/4628110 by INAF Palermo (Osservatorio Astronomico di Palermo) user on 25 September 2020

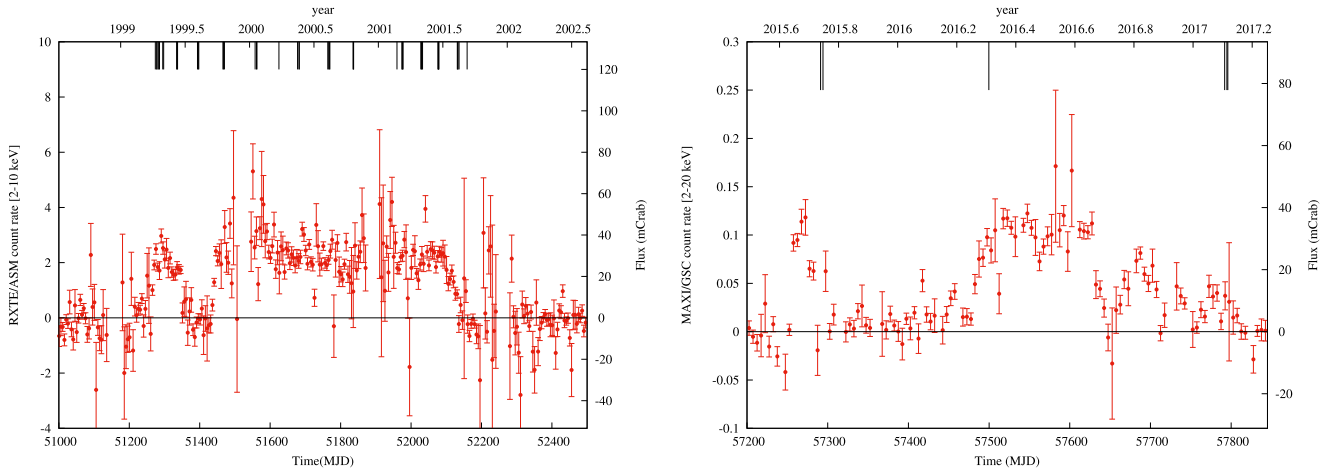

Figure 1. Light curve of MXB 1659–298 during the outburst that occurred between 1999 and 2001 (left panel) and the latest starting in 2015 (right panel). The left panel shows the *RXTE*/ASM light curve in the 2–10 keV band, the right panel shows the MAXI/GSC light curve in the 2–20 keV energy range; the bin time is five days for both light curves. The eclipse arrival times are also indicated.

we selected 43 *RXTE*/PCA observations showing the eclipse and for which it is possible to estimate the ingress and egress time accurately. To estimate the eclipse arrival times from the *RXTE*/PCA observations, we analysed the standard product background-subtracted light curves with a bin time of 0.125 s and applied the solar-system barycentric correction using the FTOOL `faxbary`.

NuSTAR (Harrison et al. 2013) observed MXB 1659–298 twice in 2015 and 2016 with the independent solid-state photon-counting detector modules (FPMA and FPMB) for 96 and 50 ks, respectively. We processed the raw (Level 1) data with the FTOOL `nupipeline` (HEASOFT version 6.19), obtaining cleaned and calibrated event data (Level 2). The solar-system barycentric corrected events of the FPMA and FPMB telescopes have been obtained by applying the tool `nuproducts` to the Level 2 data. The corresponding light curves were created by selecting a circular extraction region for the source events with a radius of 49 arcsec and using the 1.6–20 keV energy range. The persistent emission has a count rate of 2 count s^{-1}. A complete eclipse and an eclipse without ingress are observed 24 and 76 ks from the start time. The count rate during the eclipse is 0.02 count s^{-1}. The presence of the ingress to the eclipse 49.7 ks from the start time is also evident. During the second observation MXB 1659–298 is brighter, with a persistent count rate of 20 count s^{-1}; a whole eclipse is observed 30 ks after the start time of the observation. To increase the statistics of the *NuSTAR* light curve, we summed the FPMA and FPMB light curves using the FTOOL `lcmath`.

During the 2015 outburst, MXB 1659–298 was observed several times with *Swift*/XRT (Gehrels et al. 2004; Burrows et al. 2005), although only three observations show a complete eclipse. We obtained further *Swift*/XRT data as target-of-opportunity observations performed on 2017 February 8, 10 and 11 (obsids 0003400266, 0003400267 and 0003400268). All these observations cover the whole eclipse. The XRT data were processed with standard procedures (XRTPIPELINE v0.13.1) and with standard filtering and screening criteria using FTOOLS. For our timing analysis, we also converted the event arrival times to the solar-system barycentre with the tool `barycorr` and subtracted the background using the FTOOL `lcmath`.

The All-Sky monitor (ASM: Levine et al. 1996) on board *RXTE* monitored the 1999–2001 outburst (Fig. 1, left panel). The two *XMM–Newton* observations were performed at a similar ASM count rate of 2.5 count s^{-1} (about 30 mCrab in flux), corresponding to the source maximum flux. The outburst showed a sort of precursor lasting 100 d; afterwards the flux decreased to a value compatible with zero for 86 d and finally increased again, rapidly reaching a constant flux of 30 mCrab for 700 d.

The Gas Slit Camera (GSC: Mihara et al. 2011) on board the Monitor of All-sky X-ray Image (MAXI: Matsuoka et al. 2009) observed the recent outburst (see Fig. 1, right panel). The morphology of the outburst is similar to the previous one, with a sort of precursor lasting 50 d, a new quiescent stage lasting 150 d and, after that, an increase of the flux at 30 mCrab lasting 150 d. The maximum GSC count rate is 0.12 count s^{-1}. *XMM–Newton* and *NuSTAR* (obsid. 90101013002) observed the source when the GSC count rate was 0.05 count s^{-1}; *NuSTAR* observed the source a second time when MXB 1659–298 was brighter, with a corresponding GSC count rate of 0.1 count s^{-1}.

3 METHOD AND ANALYSIS

To estimate the eclipse arrival times, we folded the solar-system barycentric corrected light curves using a trial time of reference and orbital period, $T_{\rm fold}$ and P_0, respectively. The value of the adopted $T_{\rm fold}$ corresponds to a time close to the start time of the corresponding observation. The adopted value of P_0 is 7.11610872 h, corresponding to the value of the orbital period at T_0 = 43 058.72609 MJD obtained by Oosterbroek et al. (2001) adopting a quadratic ephemeris.

We fitted the eclipse profiles with a simple model consisting of a step-and-ramp function, where the count rates before, during and after the eclipse are constant and the intensity changes linearly during the eclipse transitions. This model involves seven parameters: the count rates before, during and after the eclipse, called C_1, C_2 and C_3, respectively; the phases of the start and stop times of the ingress (ϕ_1 and ϕ_2) and, finally, the phases of the start and stop times of the egress (ϕ_3 and ϕ_4). We show a typical eclipse of MXB 1659–298 in Fig. 2. The eclipse was observed during the *RXTE*/PCA observation P40050-04-16-00; the superimposed curve is the step-and-ramp best-fitting function. The phase corresponding to the eclipse arrival time $\phi_{\rm ecl}$ is estimated as $\phi_{\rm ecl} = (\phi_2 + \phi_3)/2$. The corresponding eclipse arrival time is given by $T_{\rm ecl} = T_{\rm fold} + \phi_{\rm ecl} P_0$. To be more conservative, we scaled the error associated with $\phi_{\rm ecl}$ by the

Downloaded from https://academic.oup.com/mnras/article/473/3/3490/4628110 by INAF Palermo (Osservatorio Astronomico di Palermo) user on 25 September 2020

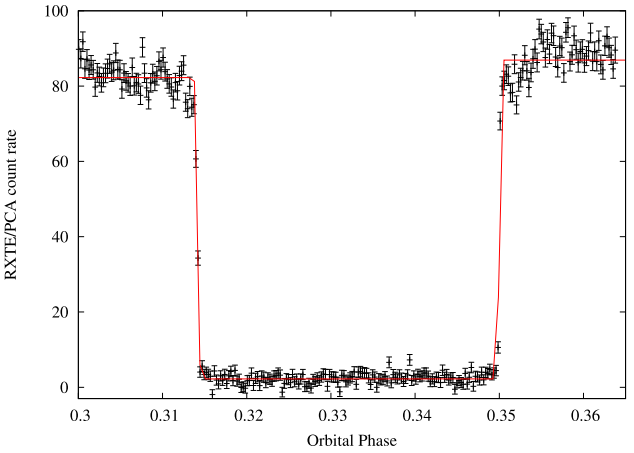

Figure 2. An eclipse of MXB 1659–628 observed by the *RXTE*/PCA instrument (observation P40050-04-16-00). The superimposed curve is the step-and-ramp function adopted to estimate the eclipse arrival time.

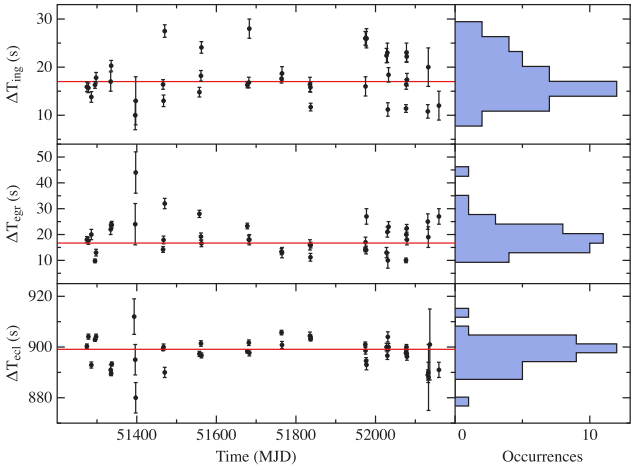

Figure 3. From top left to bottom left: the ingress, egress and eclipse duration, respectively, as a function of time. The values are obtained from the *RXTE*/PCA eclipses analysed in this work. The horizontal lines indicate the average values for each duration. From top right to bottom right: histograms of occurrences of ingress, egress and eclipse duration.

factor $\sqrt{\chi^2_{\rm red}}$ to take into account values of $\chi^2_{\rm red}$ of the best-fitting model larger than one. We show the eclipse arrival times obtained in Barycentric Dynamical Time (TDB), in units of MJD, in Table 1.

We used the 43 *RXTE*/PCA observations to estimate the average durations $\Delta T_{\rm ecl}$, $\Delta T_{\rm ing}$ and $\Delta T_{\rm egr}$ of the eclipse, the ingress and the egress, respectively. The values of $\Delta T_{\rm ecl}$, $\Delta T_{\rm ing}$ and $\Delta T_{\rm egr}$ for each eclipse are shown as a function of eclipse arrival time in Fig. 3. We found that the $\Delta T_{\rm ecl}$ values are scattered between 890 and 910 s. Fitting the values of eclipse duration with a constant, we obtained a χ^2 (d.o.f.) of 561(42) and a best-fitting value of $\Delta T_{\rm ecl} = 899.1 \pm 0.6$ s

Table 1. Journal of the X-ray eclipse arrival times of MXB 1659–298.

Point	Eclipse time (MJD; TDB)	Cycle	Delay (s)	Ref.	Point	Eclipse time (MJD; TDB)	Cycle	Delay (s)	Ref.
1	43 058.7260(2)	0	0(13)	[1],[2]	31	51 769.43726(2)	29378	107.0(1.3)	[4]
2	43 574.6441(2)	1740	26(13)	[1],[2]	32	51 835.261275(9)	29600	106.9(7)	[3]
3	51 273.978079(2)	27707	96.46(13)	[2]	33	51 836.447292(6)	29604	106.8(5)	[3]
4	51 274.571102(8)	27709	97.7(7)	[3]	34	51 837.040274(5)	29606	104.4(4)	[3]
5	51 277.832626(4)	27720	95.4(3)	[2]	35	51 960.08961(2)	30021	101(2)	[3]
6	51 278.425648(10)	27722	96.5(9)	[3]	36	51 974.321836(6)	30069	101.4(5)	[3]
7	51 281.687174(4)	27733	94.5(3)	[2]	37	51 974.914836(8)	30071	100.6(7)	[3]
8	51 283.762726(3)	27740	96.2(3)	[2]	38	51 976.397381(8)	30076	102.5(6)	[3]
9	51 285.838220(11)	27747	93.0(9)	[3]	39	51 977.286855(12)	30079	99.1(1.0)	[3]
10	51 295.029855(5)	27778	92.5(4)	[3]	40	52 027.692627(9)	30249	99.2(7)	[3]
11	51 297.698476(8)	27787	99.4(7)	[3]	41	52 029.768118(8)	30256	95.8(7)	[3]
12	51 334.464970(12)	27911	93.6(1.1)	[3]	42	52 030.954185(12)	30260	100.0(1.1)	[3]
13	51 335.650973(6)	27915	92.2(5)	[3]	43	52 032.733167(8)	30266	96.1(7)	[3]
14	51 337.133479(6)	27920	90.8(5)	[3]	44	52 076.615786(4)	30414	91.7(3)	[3]
15	51 393.46935(4)	28110	92(4)	[3]	45	52 077.208801(7)	30416	92.2(6)	[3]
16	51 396.13784(4)	28119	87(3)	[3]	46	52 077.801847(6)	30418	95.3(5)	[3]
17	51 397.32378(3)	28123	81(3)	[3]	47	52 078.394837(7)	30420	93.7(6)	[3]
18	51 466.112958(9)	28355	91.5(8)	[3]	48	52 078.987831(8)	30422	92.4(7)	[3]
19	51 467.29898(12)	28359	92.2(1.0)	[3]	49	52 131.469068(10)	30599	86.8(9)	[3]
20	51 470.264016(9)	28369	91.1(8)	[3]	50	52 132.65509(2)	30603	87(2)	[3]
21	51 557.436333(6)	28663	89.8(5)	[3]	51	52 133.24811(8)	30605	88(7)	[3]
22	51 561.290937(6)	28676	93.7(5)	[3]	52	52 136.50958(8)	30616	81(7)	[3]
23	51 562.477008(6)	28680	98.3(5)	[3]	53	52 159.34046(2)	30693	83.9(1.4)	[3]
24	51 625.03951(2)	28891	104(2)	[3]	54	57 291.24010(2)	48001	17(2)	[3]
25	51 677.817305(4)	29069	101.3(4)	[3]	55	57 294.20513(2)	48011	16(2)	[3]
26	51 681.671901(6)	29082	104.5(5)	[3]	56	57 499.682737(14)	48704	13.7(1.2)	[3]
27	51 682.857903(7)	29086	103.2(6)	[3]	57	57 792.03631(3)	49690	23(3)	[3]
28	51 763.803676(5)	29359	106.3(4)	[3]	58	57 794.70484(5)	49699	22(4)	[3]
29	51 764.989711(8)	29363	107.7(7)	[3]	59	57 795.89087 (5)	49703	23(4)	[3]
30	51 768.84426(2)	29376	106.0(1.4)	[4]					

Notes. Epoch of reference 43 058.72595 MJD, orbital period 7.11610872 h, associated errors are at 68 per cent confidence levels.
[1] Cominsky & Wood (1989), [2] Wachter et al. (2000), [3] this work, [4] Oosterbroek et al. (2001).

Downloaded from https://academic.oup.com/mnras/article/473/3/3490/4628110 by INAF Palermo (Osservatorio Astronomico di Palermo) user on 25 September 2020

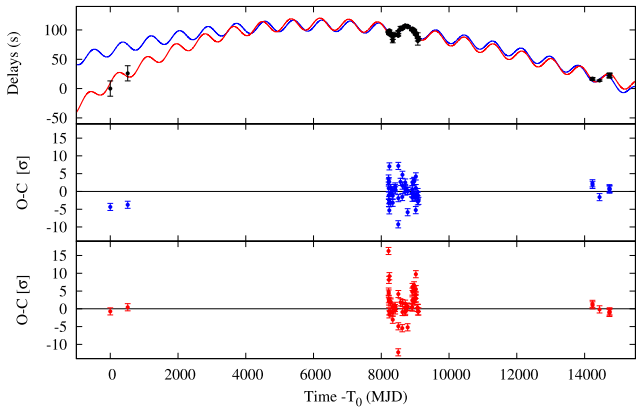

Figure 4. Top panel: delays with respect to the predicted eclipse arrival times, assuming epoch of reference $T_0 = 43\,058.72595$ MJD and orbital period $P_0 = 7.11610872$ h, plotted versus time. The two curves indicate the best-fitting functions corresponding to equations (2) and (4), respectively. Middle panel: residuals in units of σ with respect to the blue curve. Bottom panel: residuals in units of σ with respect to the red curve.

at 68 per cent confidence level (c.l.). The ingress duration is scattered between 10 and 30 s, while the egress duration is scattered between 10 and 35 s. Fitting the ingress duration values with a constant, we obtained a χ^2 (d.o.f.) of 457 (38) and a best-fitting value of $\Delta T_{\rm ing} = 17.0 \pm 0.7$ s at 68 per cent confidence level, while fitting the egress duration values we obtained a χ^2 (d.o.f.) of 560 (39) and a best-fitting value of $\Delta T_{\rm egr} = 16.7 \pm 0.9$ s at 68 per cent confidence level. The associated errors were scaled by the factor $\sqrt{\chi^2_{\rm red}}$ to take a value of $\chi^2_{\rm red}$ of the best-fitting model larger than one into account. We find that the average durations of ingress and egress are similar. We also show in Fig. 3 the occurrences of the measured ingress, egress and duration using bins of 3.1, 3.7 and 3.5 s, respectively.

We calculated the delays with respect to $P_0 = 7.11610872$ h and a reference epoch of $T_0 = 43\,058.72595$ MJD, corresponding to the first eclipse arrival time obtained by Cominsky & Wood (1989). The inferred delays, in units of seconds, of the eclipse arrival times with respect to a constant orbital period are reported in Table 1. For each point, we computed the corresponding cycle and eclipse arrival time in days with respect to the adopted T_0. We show the delays versus time in Fig. 4 (top panel).

Initially we fitted the delays with a quadratic function,

$$y(t) = a + bt + ct^2, \tag{1}$$

where t is the time in days (MJD -43058.72595), $a = \Delta T_0$ is the correction to T_0 in units of seconds, $b = \Delta P/P_0$ in units of s d^{-1}, with ΔP the correction to the orbital period, and finally $c = 1/2\,\dot{P}/P_0$ in units of s d^{-2}, with $\dot{P}$ representing the orbital period derivative. The corresponding best-fitting parameters are shown in the LQ column of Table 2. With a χ^2 of 4083 for 56 d.o.f., we note that the quadratic function does not fit the data acceptably. Since the delays seem to show a periodic modulation, we fitted them using the function

$$y(t) = a + bt + ct^2 + A \sin\left[\frac{2\pi}{P_{\rm mod}}(t - t_\phi)\right], \tag{2}$$

where A is the amplitude in seconds of the sinusoidal function, $P_{\rm mod}$ is the period of the sine function in days and, finally, t_ϕ represents the time in days at which the sinusoidal function is null. A clear improvement is obtained with a value of χ^2 (d.o.f.) of 512 (53), which translates to an F-test probability chance improvement of 7×10^{-24}. The best-fitting function, and the corresponding residuals

Table 2. Best-fitting values.

Parameter	LQ	LQS	LQCS
a (s)	-109 ± 38	65 ± 20	9 ± 29
b (s d^{-1})	0.046 ± 0.007	0.015 ± 0.004	0.037 ± 0.009
c ($\times 10^{-6}$ s d^{-2})	-2.6 ± 0.3	-1.2 ± 0.2	-4.0 ± 1.1
d ($\times 10^{-10}$ s d^{-3})	–	–	1.0 ± 0.4
A (s)	–	9.6 ± 0.6	10.2 ± 0.7
$P_{\rm mod}$ (d)	–	843 ± 7	855 ± 8
t_ϕ (d)	–	137 ± 75	-7 ± 82
χ^2(d.o.f.)	4083(56)	512(53)	455(52)

are shown in the top and middle panels of Fig. 4. The best-fitting values are shown in the third column of Table 2. The corresponding ephemeris (hereafter LQS) is

$$T_{\rm ecl}(N) = {\rm MJD(TDB)}\,43\,058.7267(2) + 0.296504580(13)N - 1.3(2) \times 10^{-12}N^2 + A \sin\left[\frac{2\pi}{N_{\rm mod}}N - \phi\right], \tag{3}$$

where N indicates the number of cycles, $N_{\rm mod} = P_{\rm mod}/P_0$ and $\phi = 2\pi t_\phi/P_{\rm mod}$. We obtained an orbital period derivative $\dot{P} = -8.5(1.2) \times 10^{-12}$ s s^{-1}, a sinusoidal modulation characterized by a periodicity $P_{\rm mod} = 2.31 \pm 0.02$ yr and a semi-amplitude $A = 9.6 \pm 0.6$ s.

It is evident that the LQS ephemeris does not predict the first two eclipse arrival times. A possible explanation is that the orbital period derivative has been changing from 1976 up to now. To take this into account, we added a cubic term to equation (2), defining the new function

$$y(t) = a + bt + ct^2 + dt^3 + A \sin\left[\frac{2\pi}{P_{\rm mod}}(t - t_\phi)\right], \tag{4}$$

where d includes the presence of a derivative of $\dot{P}$ with $d \simeq \ddot{P}/(6P)$. With the latter model, we obtain a value of χ^2 (d.o.f.) of 455 (52). By adding the cubic term, we find an F-test probability chance improvement of 0.014, indicating that the improvement of the fit is between two and three σ confidence level. The best-fitting function, and the corresponding residuals are shown in the top and bottom panels of Fig. 4. The best-fitting parameters are shown in the fourth column of Table 2. The corresponding ephemeris (hereafter LQCS) is

$$T_{\rm ecl}(N) = {\rm MJD(TDB)}\,43\,058.7261(3) + 0.296504566(3)N - 4.0(1.1) \times 10^{-12}N^2 + 3.0(1.2) \times 10^{-17}N^3 + A \sin\left[\frac{2\pi}{N_{\rm mod}}N - \phi\right], \tag{5}$$

from which we inferred the orbital period derivative at time $T_0 = 43058.7261$ MJD to be $\dot{P} = -2.7(7) \times 10^{-11}$ s s^{-1} and the orbital period second derivative $\ddot{P} = 2.4(9) \times 10^{-20}$ s s^{-2}. The sinusoidal modulation has a period $P_{\rm mod} = 2.34 \pm 0.02$ yr and a semi-amplitude $A = 10.2 \pm 0.7$ s.

4 DISCUSSION

We analysed the eclipse arrival times of MXB 1659–298, obtaining a new estimate of its ephemeris. Our baseline spans 40 years and covers the three outbursts of the source observed from 1976. We combined 51 eclipse arrival times, corresponding to the outbursts that occurred during 1999–2001 and 2015–2017, with the data already present in literature. The campaign of observations made with *Rossi-XTE*/PCA during the 1999–2001 outburst seems

Downloaded from https://academic.oup.com/mnras/article/473/3/3490/4628110 by INAF Palermo (Osservatorio Astronomico di Palermo) user on 25 September 2020

to indicate a possible periodic modulation of 2.3 yr; the delays associated with the six eclipse arrival times obtained during the most recent outburst agree with that periodic modulation. We find that the LQS ephemeris accounts for the eclipse arrival times except for the two eclipses observed during 1976–1978. The addition of a cubic term (LQCS ephemeris) allows us to account for all the available data; however, the statistical improvement is less than 3σ, suggesting that a larger baseline is needed to confirm the more complex ephemerides. In both cases, a sinusoidal modulation with a period between 840 and 860 d is needed to obtain an acceptable fit of the eclipse arrival times. In the following, we restrict our discussion to the LSQ ephemeris.

To estimate the eclipse arrival times, we fitted the shape of the eclipse using a step-and-ramp function. We used the *RXTE*/PCA observations, covering 2.4 yr during the second outburst of MXB 1659–298, to estimate the ingress/egress and eclipse durations. The obtained values are scattered; the mean values associated with the eclipse, ingress and egress are $\Delta T_{\rm ecl} = 899.1 \pm 0.6$ s, $\Delta T_{\rm ing} = 17.0 \pm 0.7$ s and $\Delta T_{\rm egr} = 16.7 \pm 0.9$ s, respectively. We find that the ingress and egress durations are similar, contrary to the reports of Cominsky & Wood (1989), who obtained ingress and egress durations of 41 ± 13 and 19 ± 13 s, respectively. Our different results can be explained by the larger sample and the higher quality of our data set.

The ingress, egress, and eclipse durations show a jittered behaviour of the order of 15 s, similar to what is observed in EXO 0748–676 (Wolff et al. 2002). Wolff, Wood & Ray (2007) discussed the possibility that magnetic activity of the companion star generates extended coronal loops above the photosphere that could explain the amplitude of the observed jitter. This scenario may be plausible, given the late K or early M-type nature of the 0.3–0.4 $M_\odot$ companion star in EXO 0748–676. Such stars can have magnetic activity if they rotate and if they have significant convective envelopes (see Wolff et al. 2007). The companion star in MXB 1659–298 is an early K-type main-sequence star (see below) and hence it likely has similar magnetic activity. Ponti et al. (2017) showed that AX J1745.6–2901 has a different phenomenology. Although jitters are observed in the ingress and egress, the eclipse duration is nearly constant. The authors suggested that the matter ejected from the accretion disc could reach the companion star with a ram pressure comparable to the pressure in the upper layers of the companion star (which is a K-type main-sequence star). This interaction could displace the atmosphere of the companion star, delaying both ingress and egress times.

4.1 Masses of the binary system

We can estimate the companion star radius from the size of its Roche lobe, which can be expressed by using the formula of Paczyński (1971):

$$R_{\rm L_2} = 0.462a \left(\frac{m_2}{m_1 + m_2} \right)^{1/3}, \quad (6)$$

where a is the orbital separation of the binary system and m_1 is the neutron-star mass in units of solar masses. Combining the previous equation with Kepler's third law, we find that

$$R_{\rm L_2} = 0.233\, m_2^{1/3} P_{\rm h}^{2/3} {\rm R}_\odot. \quad (7)$$

Assuming that the companion star fills its Roche lobe, the radius of the companion star R_2 coincides with $R_{\rm L_2}$. To estimate the mass of the companion star, we adopted the mass–radius relation for a companion star in thermal equilibrium obtained by studying cataclysmic variable systems (equation 16 in Knigge, Baraffe & Patterson 2011), although LMXBs lie in a somewhat different region of parameter space. We adopted the relation valid for large orbital periods, which is

$$R_2 = 0.293 \pm 0.010 \left(\frac{M_2}{M_{\rm conv}} \right)^{0.69 \pm 0.03} {\rm R}_\odot, \quad (8)$$

where $M_{\rm conv}$ has a value of 0.20 ± 0.02 $M_\odot$ and is the mass of the convective region of the companion star. Combining equations (7) and (8) and taking into account that the accuracy associated with the Roche-lobe radius is 2 per cent, we find that the companion star has a mass of 0.9 ± 0.3 $M_\odot$ and a radius of 0.84 ± 0.10 $R_\odot$. Hereafter, we will assume a neutron-star mass of 1.48 ± 0.22 $M_\odot$; this mass value was estimated by Özel et al. (2012) by analysing the mass distribution of neutron stars that have been recycled; the best value is the mean of the distribution and the associated error is the corresponding dispersion.

4.2 Mass-accretion rate and mass-transfer rate

Using *RXTE*/PCA data taken during the outburst in 1999, Galloway et al. (2008) observed that the flux of MXB 1659–298 peaked at $\sim 1.0 \times 10^{-9}$ erg s^{-1} cm^{-2} in the 2–25 keV energy range during 1999 April, but it was between 4×10^{-10} and 6×10^{-10} erg s^{-1} cm^{-2} throughout the remainder of the outburst. To infer a good estimation of the flux in the 0.1–100 keV energy band, we adopted the broad-band best-fitting model of the persistent spectrum obtained by Oosterbroek et al. 2001, from which we extrapolate an unabsorbed flux of 1.0×10^{-9} erg s^{-1} cm^{-2}.

From analysis of type-I X-ray bursts, the distance to MXB 1659–298 was estimated to be 9 ± 2 and 12 ± 3 kpc for hydrogen-rich and helium-rich companion stars, respectively (see Galloway et al. 2008). We assume the average of the two values, $d = 11 \pm 4$ kpc, considering that the source is accreting mixed H/He (Galloway et al. 2008).

To convert the X-ray luminosity into a mass-accretion rate, we used the relation $L_{\rm X} = \gamma \dot{M}_{\rm acc} c^2$, where γ is the efficiency of the accretion and c is the speed of the light. We take into account that the neutron star is spinning rapidly with a frequency of 567 Hz (Wijnands et al. 2001), adopting the relation proposed by Sibgatullin & Sunyaev (2000):

$$\gamma = 0.213 - 0.153\, f_{\rm kHz} + 0.02\, f_{\rm kHz}^2, \quad (9)$$

where $f_{\rm kHz}$ is the spin frequency of the neutron star in units of kHz. The latter relation is valid assuming a gravitational mass of the neutron star of 1.4 $M_\odot$ and the commonly adopted Friedman-Pandharipande-Skyrme (FPS) equation of state for a neutron star. Using a spin frequency of 567 Hz, we find that $\gamma \simeq 0.132$. Our assumption implies that all of the gravitational energy released is converted to X-ray emission and that a negligible amount of energy is carried away by bulk outflows. This is confirmed by spectral studies of the source; in fact, the absorption lines associated with the presence of Fe XXV and Fe XXVI ions are narrow, suggesting that it is not possible to associate a superluminal jet with the source (see Sidoli et al. 2001). Furthermore, Díaz Trigo & Boirin (2016) suggested that MXB 1659–298 could have a mild thermal wind, but only static atmospheres have been reported.

Using $\gamma \simeq 0.132$, we find $\dot{M}_{\rm acc} = (2.0 \pm 1.5) \times 10^{-9}$ $M_\odot$ yr^{-1}. Considering a quiescence duration of almost 14.5 yr and a mean outburst duration of 1.5 yr, we find that the average value of the observed mass-accretion rate is $|\langle \dot{M}_{\rm acc} \rangle| \simeq \dot{M}_{\rm acc} 1.5/16 = (1.9 \pm 1.4) \times 10^{-10}$ $M_\odot$ yr^{-1}.

Downloaded from https://academic.oup.com/mnras/article/473/3/3490/4628110 by INAF Palermo (Osservatorio Astronomico di Palermo) user on 25 September 2020

On the other hand, from theoretical considerations, we can estimate the rate of mass that has to be transferred from the companion star in order to explain the quadratic term of the LQS ephemeris, interpreted as the orbital period derivative of the system. From the long-term orbital evolution, we can estimate the mass-transfer rate $\dot{M}_2$ using equation (4) of Burderi et al. (2010):

$$\dot{m}_{-8} = 35(3n-1)^{-1} m_2 \left(\frac{\dot{P}_{-10}}{P_{5h}}\right), \tag{10}$$

where $\dot{m}_{-8}$ is the mass-transfer rate $\dot{M}_2$ in units of 10^{-8} $M_\odot$ yr^{-1}, n is the mass–radius index of the companion star, m_2 is the companion-star mass in units of solar masses, $\dot{P}_{-10}$ is the orbital period derivative in units of 10^{-10} s s^{-1} and P_{5h} is the orbital period in units of 5 h. This is derived by combining Kepler's third law with the contact condition, i.e. $\dot{R}_{L2}/R_{L2} = \dot{R}_2/R_2$ (where $\dot{R}_{L2}$ is the Roche-lobe radius of the secondary and R_2 is the radius of the secondary). Adopting $n = 0.69 \pm 0.03$, $m_2 = 0.9 \pm 0.3$, $\dot{P} = -8.5(1.2) \times 10^{-12}$ s s^{-1} and $P = 7.1161099(3)$ h, we find that the mass-transfer rate implied by the observed orbital period derivative is $\dot{M}_2 = -(1.8 \pm 0.7) \times 10^{-8}$ $M_\odot$ yr^{-1}, which is almost two orders of magnitude higher that the observed averaged mass-accretion rate. This means that, in order to explain the observed orbital period change rate, we have to invoke a highly non-conservative mass transfer for this system.

4.3 Prediction of the orbital period derivative for highly non-conservative mass transfer

We can define a parameter β as follows: $-\dot{M}_1 = \beta \dot{M}_2$, where $\dot{M}_1 = |\langle \dot{M}_{acc} \rangle|$ is the mass-accretion rate. Hence $\beta = 1$ in a conservative mass-transfer scenario and $\beta < 1$ in a non-conservative mass-transfer scenario. Comparing the observed averaged mass-accretion rate with the mass-transfer rate implied by the observed orbital period derivative, we obtain $\beta = 0.011 \pm 0.009$, suggesting that only $\sim$1 per cent of the mass transferred from the companion star is indeed accreted on to the neutron star.

According to theory, orbital period changes are expected to be driven by mass transfer from the companion to the compact object, by emission of gravitational waves (GR) and/or magnetic braking (MB). For orbital periods larger than two hours, the effects of MB dominate. Following Verbunt & Zwaan (1981), Verbunt (1993) and Tauris (2001), the torque associated with MB can be parametrized as

$$T_{MB} = 8.4(k^2)_{0.1} f^{-2} m_1^{-1} P_{2h}^2 q^{1/3} (1+q)^{2/3}, \tag{11}$$

where f is a dimensionless parameter for which a value of either 0.79 (Skumanich 1972) or 1.78 (Smith 1979) has been assumed, $k = 0.323$ is the gyration radius for a star with mass 0.8 $M_\odot$ (Claret & Gimenez 1990), P_{2h} is the orbital period in units of two hours, q is the mass ratio M_2/M_1 and, finally, m_1 is the mass of the compact object in units of solar masses. Because T_{MB} depends on f^{-2}, the effects of the MB on the derivative of angular momentum of the binary system will be larger for $f = 0.79$ than for $f = 1.78$.

We can calculate the secular orbital period derivative expected from the non-conservative secular evolution of the system using the relation

$$\dot{P}_{-12} = 1.37 q (1+q)^{-1/3} m_1^{5/3} P_{2h}^{-5/3} \times \left[\frac{1/3 - n}{2g(\alpha,\beta,q) - 1/3 + n}\right][1 + T_{MB}], \tag{12}$$

where

$$g(\alpha,\beta,q) = 1 - \beta q - \frac{1-\beta}{1+q}\left(\frac{q}{3} + \alpha\right) \tag{13}$$

(see Di Salvo et al. 2008; Burderi et al. 2009, 2010), where $\dot{P}_{-12}$ is the orbital period derivative in units of 10^{-12} s s^{-1} and α is a dimensionless parameter that quantifies the specific angular momentum of the ejected matter in the case of a non-conservative mass-transfer scenario. The specific angular momentum, l_{ej}, with which the transferred mass is lost from the system can be written in units of the specific angular momentum of the secondary, i.e. $\alpha = l_{ej}/(\Omega_{orb} r_2^2) = l_{ej} P (M_1 + M_2)^2/(2\pi a^2 M_1^2)$, where r_2 is the distance of the secondary star from the centre of mass of the system, a is the orbital separation and P is the orbital period of the binary system. For a neutron-star mass of 1.48 ± 0.22 $M_\odot$, we obtain an orbital period derivative of $-(6 \pm 3) \times 10^{-12}$ s s^{-1}, which is compatible within one σ with the value $\dot{P} = -(8.5 \pm 1.2) \times 10^{-12}$ s s^{-1} inferred from the eclipse arrival times.

Highly non-conservative mass transfer may be justified by the fact that MXB 1659–298 is a fast-spinning neutron star (Wijnands et al. 2001). During quiescent periods, if the region around the neutron star is free from matter up to the light-cylinder radius, the radiation pressure of the rotating magnetic dipole, given by the Larmor formula, may be able to eject from the system the matter transferred by the companion star at the inner Lagrangian point, according to the *radio ejection* mechanism as described in detail by Burderi et al. (2001). Once significant temporary reduction of the mass-accretion rate occurs, the neutron star can emit as a magnetic-dipole rotator and the radiation pressure from the pulsar may be able to eject matter out of the system. We note that the disc instability model (see the review of Lasota 2001) may have a role in triggering the *radio ejection* and starting a non-conservative mass transfer. The *radio ejection* has been invoked to explain the high orbital period derivative observed in the accreting millisecond pulsar (AMSP) SAX J1808.4–3658 (see Di Salvo et al. 2008; Burderi et al. 2009) and, more recently, for the AMSP SAX J1748.9–2021, for which a high orbital period derivative is also observed (Sanna et al. 2016). We therefore suggest that a similar mechanism could also be at work for MXB 1659–298.

The above-described scenario assumes a mass-transfer rate of $\dot{M}_2 = -(1.8 \pm 0.7) \times 10^{-8}$ $M_\odot$ yr^{-1} and a companion-star mass of 0.9 ± 0.3 $M_\odot$. The time-scale associated with the mass-transfer rate, $\tau_{\dot{M}} = M_2/|\dot{M}_2|$, is $(5.1 \pm 2.7) \times 10^7$ yr. The companion star is in thermal equilibrium if $\tau_{\dot{M}}$ is longer than the thermal time-scale $\tau_{KH} = GM_2^2/(R_2 L_2)$ of the companion star (Paczyński 1971). To estimate the thermal time-scale, we need to infer the luminosity L_2 of the companion star. For a star close to the lower main sequence, the relation $L_2/L_\odot = (M_2/M_\odot)^4$ holds (see Salaris & Cassisi 2005). Since the companion-star mass is 0.9 ± 0.3 $M_\odot$, we obtain that $\tau_{KH} = (5 \pm 3) \times 10^7$ yr which is comparable with $\tau_{\dot{M}}$. Since the two time-scales are comparable, we cannot exclude the possibility that the companion star is out of thermal equilibrium; hence, the value of 0.9 ± 0.3 $M_\odot$ has to be considered an upper limit to the companion-star mass.

We note that, for a mass of the companion star lower than 0.9 $M_\odot$, the mass-transfer rate would be also lower, because of the linear dependence of $\dot{M}_2$ on m_2 in equation (10). Therefore, the minimum mass-transfer rate is reached for $m_2 = 0.35$ $M_\odot$. This has to be considered as a lower limit to the mass of the companion, since below this mass the companion star is expected to become fully convective and magnetic braking switches off (Rappaport, Verbunt & Joss 1983). For this limiting mass, the mass-transfer

Downloaded from https://academic.oup.com/mnras/article/473/3/3490/4628110 by INAF Palermo (Osservatorio Astronomico di Palermo) user on 25 September 2020

rate is $(7 \pm 3) \times 10^{-9}$ $M_\odot$ yr^{-1}. However, a detailed study of the evolution of this system is beyond the aims of this article. Here we note that the results presented in this article do not change significantly on adopting a lower mass for the companion star. Therefore, we will continue our discussion assuming a companion-star mass of 0.9 ± 0.3 $M_\odot$, keeping in mind that lower masses for the companion star are also possible.

4.3.1 Changes of equivalent hydrogen column density N_H *during X-ray quiescence*

The mass ejected from the system can explain the variable equivalent hydrogen column density N_H measured during X-ray quiescence of the source. Cackett et al. (2008, 2013) measured two different N_H values of $(2.0 \pm 0.1) \times 10^{21}$ and $(4.7 \pm 1.3) \times 10^{21}$ cm^{-2}, respectively, at different times, while the estimation of N_H obtained by Dickey & Lockman (1990) is 1.8×10^{21} cm^{-2}. Here, we suggest that the matter ejected from the system can account for the additional absorption. Most of the matter provided by the companion is ejected from the inner Lagrangian point, forming a circumbinary ring of matter around MXB 1659–298. Because of the large inclination angle of the system, it is possible that the ejected matter interposes itself between the source and the observer. Local density inhomogeneities and/or changes in the mass-transfer rate could produce changes in the equivalent hydrogen column, as observed by Cackett et al. (2008, 2013) during quiescence.

We use equation (4) of Iaria et al. (2013) to estimate the density of the ejected matter:

$$n(r) \simeq 6.9 \times 10^{11}(1-\beta)\zeta^{-1}\eta^{-1}\dot{m}_E(m_1+m_2)^{-1}P_h^{-1}\left(\frac{r}{a}\right)^{-3/2}, \quad (14)$$

where $n(r)$ is the density in units of cm^{-3}, r is the distance from the inner Lagrangian point, ζ is a parameter that takes into account a non-spherical distribution of matter, η a parameter larger than 1, $\dot{m}_E$ is the mass-transfer rate in units of Eddington mass-accretion rate and a is the orbital separation of the binary system. Adopting a mass-transfer rate of $|\dot{M}_2| = (1.8 \pm 0.7) \times 10^{-8}$ $M_\odot$ yr^{-1}, an orbital period of 7.116 h and companion-star and neutron-star masses of 0.9 ± 0.3 $M_\odot$ and 1.48 ± 0.22 $M_\odot$, respectively, we obtain $n(a) = (5 \pm 2) \times 10^{10}(\zeta\eta)^{-1}$ cm^{-3}. Supposing a constant particle density along the line of sight, we can determine the equivalent hydrogen column density N_H associated with neutral matter using $N_H = n(a) \times a$, where $a = (1.74 \pm 0.10) \times 10^{11}$ cm. We find $N_H = (8 \pm 4) \times 10^{21}(\zeta\eta)^{-1}$ cm^{-2}. Since the quantity $\zeta\eta$ is close to unity (see Iaria et al. 2013), we find that the equivalent hydrogen column of cold matter is $N_H = (8 \pm 4) \times 10^{21}$ cm^{-2}, which is of the same order of magnitude as the changes observed during quiescence of the source and, furthermore, explains the discrepancy of a factor of two between the N_H values measured by Cackett et al. (2013) and Dickey & Lockman (1990).

4.3.2 Inclination angle of the source

From our estimate of the duration of the eclipse ingress, $\Delta T_{ing} \simeq 17$ s, we can estimate the size of the corona, R_c, surrounding the central source using the relation

$$\frac{2\pi}{P}a = \frac{2R_c}{\Delta T_{ing}}. \quad (15)$$

We find $R_c = (3.6 \pm 0.3) \times 10^8$ cm. Assuming a neutron-star mass of 1.48 ± 0.22 $M_\odot$ and a companion-star mass of 0.9 ± 0.3 $M_\odot$, we infer that the Roche-lobe radius, R_{L_1}, of the compact object is 5.8×10^{10} cm. The radius of the accretion disc, R_d, corresponds to the tidal radius $R_T \simeq 0.9R_{L_1}$ (see Frank, King & Raine 2002, equation 5.122), hence the accretion disc radius is $R_d \simeq 5.3 \times 10^{10}$ cm. This result suggests that the corona is much smaller than the accretion disc and therefore it is a relatively compact corona around the neutron star.

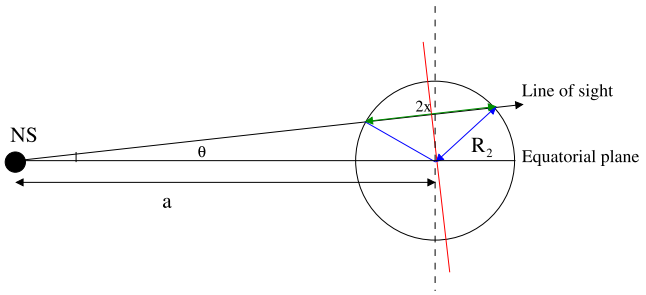

Figure 5. Schematic geometry of MXB 1659–298, not to scale.

Using our estimate of the eclipse duration, we can also estimate the inclination angle, $i = 90^\circ - \theta$, of the system, finding the angle θ represented in Fig. 5. Knowing that the eclipse duration is $\Delta T_{ecl} \simeq 899.1$ s, we can estimate the size of the occulted region x as before, using

$$\frac{2\pi}{P}a = \frac{2x}{\Delta T_{ecl}}. \quad (16)$$

We obtain $x = (1.92 \pm 0.11) \times 10^{10}$ cm, where $2x$ is the segment shown in Fig. 5. The angle θ, representing the angle between the line of sight and the equatorial plane of MXB 1659–298, is obtained from

$$\tan\theta = \left[\frac{R_2^2 - x^2}{a^2 - (R_2^2 - x^2)}\right]^{1/2}.$$

We infer $i = 72^\circ \pm 3^\circ$. Our result is compatible with the presence in the light curve of the source of dips and total eclipses, which can be observed for inclination angles in the approximate range 75°–80° (see fig. 5.10 of Frank et al. 2002). We note that, for a companion-star mass of 0.35 $M_\odot$, the inclination angle of the system is $76.0^\circ \pm 0.7^\circ$, which is marginally compatible with the value obtained for a companion-star mass of 0.9 ± 0.3 $M_\odot$.

Sidoli et al. (2001) detected absorption lines associated with the presence of O VIII, Ne IX, Fe XXV and Fe XXVI ions in the XMM spectrum of MXB 1659–298. The authors, assuming an inclination angle of 80°, inferred the distance of the absorbing plasma from the central source, finding $r_{Fe} \lesssim 2.4 \times 10^8$ cm, $r_O \gtrsim 3 \times 10^8$ cm and $r_{Ne} \gtrsim 9 \times 10^7$ cm, respectively. Revisiting the results obtained by Sidoli et al. (2001), for an inclination angle of 72° we find $r_{Fe} \lesssim 8 \times 10^8$ cm, $r_O \gtrsim 1 \times 10^9$ cm and $r_{Ne} \gtrsim 3 \times 10^8$. Since we have estimated the size of the corona $R_c \simeq 3.6 \times 10^8$ cm, we suggest that the absorbing plasma is located in the outer regions of the corona.

4.4 The 2.31-yr periodic modulation: possible explanations

Our ephemeris of MXB 1659–298 also includes a sinusoidal modulation with a period of 2.31 ± 0.02 yr. This periodic modulation might be produced by the gravitational coupling of the orbit with changes in the shape of the magnetically active companion star. These changes are thought to be a consequence of the torque applied by the magnetic activity of a subsurface magnetic field

Downloaded from https://academic.oup.com/mnras/article/473/3/3490/4628110 by INAF Palermo (Osservatorio Astronomico di Palermo) user on 25 September 2020

in the companion star interacting with the convective envelope. The convective envelope induces a cyclic exchange of angular momentum between the inner and outer regions of the companion star, causing a change in the gravitational quadrupole moment (see Applegate 1992; Applegate & Shaham 1994). A similar mechanism has been proposed for the eclipsing LMXBs EXO 0748–676 (Wolff et al. 2009) and AX J1745.6–2901 (Ponti et al. 2017).

The inferred periodicity of 843 d and amplitude of 9.6 s correspond in this case to an orbital period variation of $\Delta P/P = (8.3 \pm 0.5) \times 10^{-7}$. We estimate that the transfer of angular momentum needed to produce an orbital period change ΔP is $\Delta J \simeq 3.8 \times 10^{46}$ g cm^2 s^{-1} (see Applegate 1992, equation 27 therein). The asynchronism of the companion, quantified through the quantity $\Delta\Omega/\Omega$, is 3.7×10^{-4}, where Ω is the orbital angular velocity of the binary system and $\Delta\Omega$ is the variation of the orbital angular velocity needed to produce ΔP (see Applegate & Shaham 1994, equation 3 therein). The variable part of the luminosity of the companion star required to power the gravitational quadrupole changes is $\Delta L \simeq 1.5 \times 10^{32}$ erg s^{-1}. Considering that $L_2/\mathrm{L}_\odot = (M_2/\mathrm{M}_\odot)^4$, we obtain $\Delta L/L_2 = 0.06 \pm 0.10$, in agreement with the prediction of $\Delta L \simeq 0.1L$ obtained for magnetic active stars (see Applegate 1992 and references therein). Our results suggest that a change in the magnetic quadrupole of the companion star can produce the observed sinusoidal modulation. The energy required to transfer angular momentum from the interior of the companion star to a thin shell, with mass 10 per cent of M_2, at the surface (and vice versa) is furnished by 10 per cent of the thermonuclear energy produced by the companion star. Furthermore, we obtain that the mean subsurface magnetic field B of the companion star is close to 1×10^5 G (see Applegate 1992, equation 23 therein).

The origin of the sinusoidal modulation could alternatively be explained by the presence of a third body orbiting around the binary system, similar to what is found for the LMXB XB 1916–053 (Iaria et al. 2015b). Adopting an inclination angle of 72°.1, we find that the orbital separation between the centre of mass of MXB 1659–298 and the centre of mass of the triple system is $a_\mathrm{x} \sin i = Ac$, where c is the speed of light. Using the values in the third column of Table 2, we obtain that $a_\mathrm{x} \sin i = (2.9 \pm 0.2) \times 10^{11}$ cm. Assuming a non-eccentric and coplanar orbit of the third body and that the companion star is in thermal equilibrium, the mass M_3 of the third body is obtained from

$$\frac{M_3 \sin i}{(M_3 + M_\mathrm{bin})^{2/3}} = \left(\frac{4\pi^2}{G}\right)^{1/3} \frac{Ac}{P_\mathrm{mod}^{2/3}}, \tag{17}$$

where $\mathrm{M_{bin}}$ is the mass of the binary system and P_mod is the revolution period of the third body around the binary system (see e.g. Bozzo et al. 2007). We obtain that the mass of the third body is $22 \pm 3M_\mathrm{J}$, where M_J indicates the Jovian mass; the distance of the third body from the centre of mass of the triple system is 2.3 ± 0.3 au. Releasing the constraint of a co-planar orbit, the mass of the third body is larger than $21M_\mathrm{J}$. We have checked that the derived orbit of the third body is stable in the formalism of Kiseleva, Eggleton & Orlov (1994). If this result is confirmed, this will be the first circumbinary Jovian planet spotted around an LMXB. In the case of a no-coplanar orbit, we find that the mass of the third body should be larger than $21M_\mathrm{J}$.

5 CONCLUSIONS

We have estimated 51 eclipse arrival times for MXB 1659–298 when the source was in outburst in 2000, 2001 and 2015, using *Rossi-XTE*, *XMM–Newton*, *NuSTAR* and *Swift*/XRT data. In combination with the values reported in the literature, we obtain a baseline of 40 years, from 1976–2017, to constrain the ephemeris of the source. The data are clustered in three temporal intervals covering six years, corresponding to the periods when the source was in outburst. Under the hypothesis that the companion star is in thermal equilibrium and fills its Roche lobe, we estimate that the companion-star mass is 0.9 ± 0.3 $\mathrm{M}_\odot$, in agreement with the possibility that the companion is an early K-type main-sequence star, as reported in the literature.

Using *RXTE*/PCA data, we have studied the profile of the total eclipse, observing jitters in the ingress/egress duration and eclipse duration of about 10–15 s. The average values of the ingress, egress and eclipse durations are 17.0 ± 0.7, 16.7 ± 0.9 and 899.1 ± 0.6 s, respectively. Using the average ingress and eclipse duration values, we find that the size of the corona surrounding the neutron star is $R_\mathrm{c} = (3.6 \pm 0.3) \times 10^8$ cm and the inclination angle of the binary system is $72^\circ \pm 3^\circ$, assuming a companion star in thermal equilibrium.

We find that the eclipse arrival times are well described by an ephemeris composed of a linear, a quadratic and a sinusoidal term. We find an orbital period derivative of $\dot{P} = -8.5(1.2) \times 10^{-12}$ s s^{-1}. We are able to explain the value of $\dot{P}$ assuming a highly non-conservative mass-transfer scenario. We find that the mass-transfer rate is $\dot{M}_2 = -(1.8 \pm 0.7) \times 10^{-8}$ $\mathrm{M}_\odot$ yr^{-1} and only 1 per cent of this mass is observed to accrete on to the neutron star. We also suggest that the ejected matter produces a local absorber with an equivalent hydrogen column density of $(8 \pm 4) \times 10^{21}$ cm^{-2}.

The sinusoidal modulation has a period of 2.31 ± 0.02 yr and an amplitude of 9.6 ± 0.6 s. The 2.3-yr periodic modulation of the orbital period can be explained by the presence of either a gravitational quadrupole coupling of the orbit to a variable deformation of the magnetically active companion star or a third body orbiting around the binary system. In the second scenario, we find that the mass of the third body is larger than $21M_\mathrm{J}$.

Finally, we note that the first two eclipse arrival times, measured during the outburst that occurred in 1976–1978, are marginally accounted for using the quadratic ephemeris. To fit them, we adopted a more complex ephemeris, taking into account the second derivative of the orbital period. However, the statistical improvement is smaller than 3σ. A larger baseline is needed to confirm or discard a more complex function to account for the ephemeris.

ACKNOWLEDGEMENTS

This research has made use of data and/or software provided by the High Energy Astrophysics Science Archive Research Center (HEASARC), which is a service of the Astrophysics Science Division at NASA/GSFC and the High Energy Astrophysics Division of the Smithsonian Astrophysical Observatory. This research has made use of MAXI data provided by RIKEN, JAXA and the MAXI team.We are grateful to the *Swift* team, and especially Kim Page, for their assistance and flexibility in the scheduling of our ToO observations. This work was partially supported by the Regione Autonoma della Sardegna through POR-FSE Sardegna 2007-2013, L.R. 7/2007, Progetti di Ricerca di Base e Orientata, Project No. CRP-60529. We also acknowledge a financial contribution from the agreement ASI-INAF I/037/12/0. AR and AS gratefully acknowledge the Sardinia Regional Government for its financial support (POR Sardegna FSE Operational Programme of the Autonomous Region of Sardinia, European Social Fund 2007–2013 – Axis IV Human Resources, Objective l.3, Line of Activity l.3.1.). We also

Downloaded from https://academic.oup.com/mnras/article/473/3/3490/4628110 by INAF Palermo (Osservatorio Astronomico di Palermo) user on 25 September 2020

acknowledge fruitful discussions with the international team on 'The disc magnetosphere interaction around transitional ms pulsars', supported by ISSI (International Space Science Institute), Bern.

REFERENCES

Applegate J. H., 1992, ApJ, 385, 621
Applegate J. H., Shaham J., 1994, ApJ, 436, 312
Bahramian A., Heinke C. O., Wijnands R., Degenaar N., 2016, Astron. Tel., 8699
Bozzo E. et al., 2007, A&A, 476, 301
Burderi L. et al., 2001, ApJ, 560, L71
Burderi L., Riggio A., di Salvo T., Papitto A., Menna M. T., D'Aì A., Iaria R., 2009, A&A, 496, L17
Burderi L., Di Salvo T., Riggio A., Papitto A., Iaria R., D'Aì A., Menna M. T., 2010, A&A, 515, A44
Burrows D. N. et al., 2005, Space Sci. Rev., 120, 165
Cackett E. M., Wijnands R., Miller J. M., Brown E. F., Degenaar N., 2008, ApJ, 687, L87
Cackett E. M., Brown E. F., Cumming A., Degenaar N., Fridriksson J. K., Homan J., Miller J. M., Wijnands R., 2013, ApJ, 774, 131
Chou Y., 2014, Res. Astron. Astrophys., 14, 1367
Claret A., Gimenez A., 1990, Ap&SS, 169, 215
Cominsky L. R., Wood K. S., 1984, ApJ, 283, 765
Cominsky L. R., Wood K. S., 1989, ApJ, 337, 485
Cominsky L., Ossmann W., Lewin W. H. G., 1983, ApJ, 270, 226
Di Salvo T., Burderi L., Riggio A., Papitto A., Menna M. T., 2008, MNRAS, 389, 1851
Díaz Trigo M., Boirin L., 2016, Astron. Nachr., 337, 368
Díaz Trigo M., Parmar A. N., Boirin L., Méndez M., Kaastra J. S., 2006, A&A, 445, 179
Dickey J. M., Lockman F. J., 1990, ARA&A, 28, 215
Filippenko A. V., Leonard D. C., Matheson T., Li W., Moran E. C., Riess A. G., 1999, PASP, 111, 969
Frank J., King A., Raine D. J., 2002, Accretion Power in Astrophysics: Third Edition. Cambridge Univ. Press, Cambridge, UK
Galloway D. K., Muno M. P., Hartman J. M., Psaltis D., Chakrabarty D., 2008, ApJS, 179, 360
Gehrels N. et al., 2004, ApJ, 611, 1005
Harrison F. A. et al., 2013, ApJ, 770, 103
Iaria R., di Salvo T., Burderi L., D'Aí A., Papitto A., Riggio A., Robba N. R., 2011, A&A, 534, A85
Iaria R., Di Salvo T., D'Aì A., Burderi L., Mineo T., Riggio A., Papitto A., Robba N. R., 2013, A&A, 549, A33
Iaria R. et al., 2015a, A&A, 577, A63
Iaria R. et al., 2015b, A&A, 582, A32
in't Zand J., Heise J., Smith M. J. S., Cocchi M., Natalucci L., Celidonio G., Augusteijn T., Freyhammer L., 1999, IAU Circ., 7138
Jahoda K., Swank J. H., Giles A. B., Stark M. J., Strohmayer T., Zhang W., Morgan E. H., 1996, in Siegmund O. H., Gummin M. A., eds, Proc SPIE Vol. 2808, EUV, X-Ray, and Gamma-Ray Instrumentation for Astronomy VII. SPIE, Bellingham, p 59
Jansen F. et al., 2001, A&A, 365, L1
Kiseleva L. G., Eggleton P. P., Orlov V. V., 1994, MNRAS, 270, 936
Knigge C., Baraffe I., Patterson J., 2011, ApJS, 194, 28
Lasota J.-P., 2001, New Astron Rev., 45, 449
Levine A. M., Bradt H., Cui W., Jernigan J. G., Morgan E. H., Remillard R., Shirey R. E., Smith D. A., 1996, ApJ, 469, L33
Lewin W. H. G., Hoffman J. A., Doty J., Liller W., 1976, IAU Circ., 2994
Matsuoka M. et al., 2009, PASJ, 61, 999
Mihara T. et al., 2011, PASJ, 63, S623
Negoro H. et al., 2015, Astron. Tel., 7943
Oosterbroek T., Parmar A. N., Sidoli L., in't Zand J. J. M., Heise J., 2001, A&A, 376, 532
Özel F., Psaltis D., Narayan R., Santos Villarreal A., 2012, ApJ, 757, 55
Paczyński B., 1971, ARA&A, 9, 183
Ponti G., De K., Muñoz-Darias T., Stella L., Nandra K., 2017, MNRAS, 464, 840
Rappaport S., Verbunt F., Joss P. C., 1983, ApJ, 275, 713
Salaris M., Cassisi S., 2005, Evolution of Stars and Stellar Populations. Wiley, New York
Sanna A. et al., 2016, MNRAS, 459, 1340
Sibgatullin N. R., Sunyaev R. A., 2000, Astron. Lett., 26, 699
Sidoli L., Oosterbroek T., Parmar A. N., Lumb D., Erd C., 2001, A&A, 379, 540
Skumanich A., 1972, ApJ, 171, 565
Smith M. A., 1979, PASP, 91, 737
Strüder L. et al., 2001, A&A, 365, L18
Tauris T. M., 2001, in Podsiadlowski P., Rappaport S., King A. R., D'Antona F., Burderi L., eds, ASP Conf. Ser. Vol. 229, Evolution of Binary and Multiple Star Systems. Astron. Soc. Pac., San Francisco, p. 145
Verbunt F., 1993, ARA&A, 31, 93
Verbunt F., 2001, A&A, 368, 137
Verbunt F., Zwaan C., 1981, A&A, 100, L7
Wachter S., Smale A. P., Bailyn C., 2000, ApJ, 534, 367
Warner B., 1995, Cataclysmic Variable Stars, Cambridge Astrophysics Series. Cambridge Univ. Press, Cambridge
Wijnands R., Strohmayer T., Franco L. M., 2001, ApJ, 549, L71
Wijnands R., Nowak M., Miller J. M., Homan J., Wachter S., Lewin W. H. G., 2003, ApJ, 594, 952
Wolff M. T., Hertz P., Wood K. S., Ray P. S., Bandyopadhyay R. M., 2002, ApJ, 575, 384
Wolff M. T., Wood K. S., Ray P. S., 2007, ApJ, 668, L151
Wolff M. T., Ray P. S., Wood K. S., Hertz P. L., 2009, ApJS, 183, 156

This paper has been typeset from a TEX/LATEX file prepared by the author.

Downloaded from https://academic.oup.com/mnras/article/473/3/3490/4628110 by INAF Palermo (Osservatorio Astronomico di Palermo) user on 25 September 2020